applied sciences

MDPI

*Article*

# High Reliability Evaluation and Lifetime Prediction of 50 GHz Athermal AWG Module

**Kwang-Su Yun [1,2], Chong-Hee Yu [1], Kwon-Seob Lim [1], Young-Sic Kim [3] and Insu Jeon [2,*]**

[1] AI Convergence Research Section, Electronics and Telecommunications Research Institute, Gwangju 34129, Korea; yks0604@etri.re.kr (K.-S.Y.); yuch@etri.re.kr (C.-H.Y.); kaide.lim@etri.re.kr (K.-S.L.)
[2] Department of Mechanical Engineering, Chonnam National University, 77 Yongbong-ro, Buk-gu, Gwangju 61186, Korea
[3] PPI Inc., 958-10 Dae-chon dong, Buk-gu, Gwangju 61008, Korea; yskim@ppitek.com
* Correspondence: i_jeon@chonnam.ac.kr; Tel.: +82-62-530-1688

**Abstract:** A 96-channel (50 GHz-spacing) athermal AWG has been developed. It has a wide operating range due to reduced temperature dependence than conventional AWG. The temperature dependence of the center wavelength of the developed module satisfied the ±0.05 nm range in all channels in the temperature range of −40 °C to 85 °C, and the insertion loss variation was also less than ±0.5 dB. As a result of validating its reliability through tests based on Telcordia-GR-1209 and GR-1221, the temperature dependence of the center wavelength satisfied the ±0.022 nm range, and the insertion loss variation was also less than ±0.2 dB. Accelerated life testing showed an expected service life of over 36.7 years, ensuring long-term safety of communication quality in harsh indoor and outdoor environments.

**Keywords:** accelerated test; athermal; DWDM; lifetime prediction; reliability



**Citation:** Yun, K.-S.; Yu, C.-H.; Lim, K.-S.; Kim, Y.-S.; Jeon, I. High Reliability Evaluation and Lifetime Prediction of 50 GHz Athermal AWG Module. *Appl. Sci.* **2021**, *11*, 11107. https://doi.org/10.3390/app112311107

Academic Editor: Jeong-Geun Kim

Received: 10 October 2021
Accepted: 18 November 2021
Published: 23 November 2021



## 1. Introduction

Mobile data traffic continues to increase. Mobile data speed increased from 200 kbps to several Gbps with the transition from 3G over LTE and LTE-A to 5G, and the number of users, antennas, and base stations is increasing exponentially [1]. Low-power multi-channel photonic integrated devices are promising candidates to address the increasing energy consumption and bandwidth demands faced by network operators, and enable efficient deployment of wavelength division multiplexing (WDM) in next-generation passive optical networks (PON) [2,3].

DWDM (dense wavelength division multiplexing) [4–7] has expanded from long-distance transmission systems to large cities and access networks for many years to meet the rapid advancement, diversification, acceleration, and the large-capacity of communication services based on Internet technologies. In particular, arrayed waveguide grating (AWG) [8] fabricated using polymeric optical waveguides is playing an increasingly significant role in DWDM systems.

Compared to temperature control circuits adopting typical AWGs, the athermal AWGs do not require a power supply. Therefore, thermal AWGs are suitable for use in WDM-PON, VMUX, ROADM, and OXC. DWDM systems are used because of their support for multiple channels, low insertion loss [9], small device size, high stability, and integration with other polymer devices. A wide variety of studies have been conducted on fabricating AWGs in Korea and other countries, and most of them have focused on temperature compensation techniques using the thermal expansion coefficient of metals [10–15]. The center wavelength of the output end of an AWG wavelength division multiplexing device fabricated with conventional silica-based PLC (planar lightwave circuits) technologies has a temperature dependence of about 0.011 nm/°C [10,16], which causes crosstalk between channels, so the temperature of the device needs to be stabilized when applied to DWDM

systems. However, for active temperature stabilization, the use of cooling devices such as heaters or Peltier Coolers requires power consumption and electronic control circuits, and issues such as price, device size, and reliability limit the widespread use of DWDM systems [17,18].

This study performed reliability and accelerated life tests on a 96-channel (50 GHz-spacing) athermal AWG module fabricated by installing a temperature compensation board on the back of a silicon substrate. We tried to verify the reliability for stabilizing the communication quality in the network environment and predict the life by checking the life of more than 10 years [19] required for optical communication parts.

## 2. The Principle of Temperature Independence

### *2.1. Principle of AWG*

Figure 1 shows the waveguide circuit structure of an arrayed waveguide grating (AWG), in which input waveguides, input slab waveguides, arrayed waveguides, output slab waveguides, and output waveguides are arranged on a substrate. The optical demultiplexer operates as follows. When a WDM signal containing multiple optical signals with wavelengths $\lambda_1$~$\lambda_n$ enters the input waveguides, it is diffracted and diffused by the input slab waveguide and transmitted to the arrayed waveguide. This signal consists of waveguides placed side by side in each waveguide. The signal emitted from the input slab waveguide propagates, and adjacent waveguides are placed at a fixed optical path length difference of ΔL. Therefore, the signals propagating from each waveguide show a phase difference. Signals passing through the arrayed waveguide enter the output slab waveguide and are diffracted and diffused, but the signals passing through each waveguide interfere with each other and are virtually all diffracted in the direction where the wavefronts are aligned. The phase condition in which the wavefronts are aligned is as follows.

$$n_s\, D \sin \varnothing + n_c \Delta \mathrm{L} = m\lambda \tag{1}$$

where $n_c$ is the effective index of arrayed waveguides and $n_s$ is the effective index of refraction of slab waveguides; $\varnothing$ is the diffraction angle; $D$ is the distance between the arrayed waveguides; $\lambda$ is the wavelength; and $m$ is an arbitrary integer and the order of diffraction.

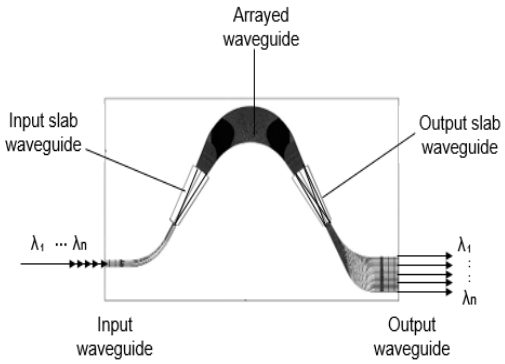


**Figure 1.** Light waveguide circuit structure of AWG.

Therefore, signals with different wavelengths converge at different points at the output port of the output slab waveguide, and by placing an output waveguide at each of these points, signals with different wavelengths can be sent to different waveguides to extract signals with wavelengths $\lambda_1$~$\lambda_n$.

### *2.2. Temperature Dependence of the Center Wavelength*

As described above, an AWG is used to multiplex and demultiplex signals of a set wavelength, but this wavelength (center wavelength) changes according to temperature. The refractive index of the waveguide material changes as the temperature changes, and

the substrate and waveguide expand or contract, changing the length of the optical path. As a result, the focal position shifts in the input of the input slab waveguide, and the wavelength of the signal entering the input waveguide changes. In Equation (1), setting $\phi$ to zero and differentiating the differential equation with respect to $\lambda$ by temperature $T$ expresses the center wavelength's magnitude of temperature dependence.

$$n_c \Delta \mathrm{L} = m\lambda \tag{2}$$

$$\frac{dn_C}{dT}\Delta \mathrm{L} + n_c \frac{d(\Delta \mathrm{L})}{dT} = m\frac{d\lambda}{dT} \tag{3}$$

$$\begin{aligned} \frac{d\lambda}{dT} &= \frac{1}{m}\left(\frac{dn_C}{dT}\Delta \mathrm{L} + n_c \frac{d(\Delta \mathrm{L})}{dT}\right) \\ &= \lambda\left(\frac{1}{n_c}\frac{dn_C}{dT} + \frac{1}{\Delta \mathrm{L}}\frac{d(\Delta \mathrm{L})}{dT}\right) \\ &= \frac{\lambda}{n_c}\frac{dn_C}{dT} + \lambda\alpha_s \end{aligned} \tag{4}$$

where $\alpha_s = \frac{1}{\Delta \mathrm{L}}\frac{d(\Delta \mathrm{L})}{dT}$ is the substrate's coefficient of expansion for silicon.

Since the coefficient of thermal expansion of the substrate is much greater than that of the waveguide, the coefficient of thermal expansion of the substrate was applied.

The first term to the right of the equation represents the temperature dependence of the refractive index, and the second term is the change in refractive index caused by the stress applied to the waveguide due to changes in the waveguide path's length as the material shrinks or expands. The temperature dependence of the silica glass refractive index is $8 \times 10^{-6}/^{\circ}\mathrm{C}$, and the substrate's coefficient of expansion is $3 \times 10^{-6}/^{\circ}\mathrm{C}$ (for silicon, $\alpha_s$), so the change in center wavelength is about 0.011 nm/°C.

### *2.3. Principle of Temperature Compensation*

This study focused on the linear dispersion of AWG to compensate for this temperature dependence. Figure 2 shows the input slab waveguide of AWG.

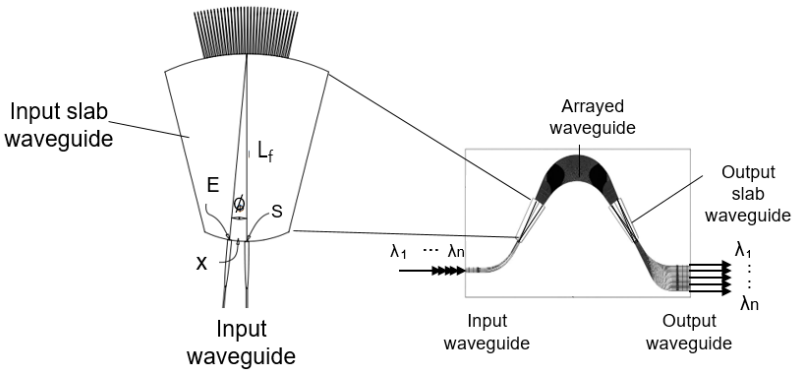


**Figure 2.** Input slab waveguide of AWG.

The symbol S corresponds to the position when Ø = 0 and wavelength $\lambda_0$ in Equation (1), and is expressed as follows under these conditions.

$$\mathrm{x}\, n_s \frac{D}{L_f} + n_C \Delta \mathrm{L} = \mathrm{m}\lambda \tag{5}$$

$$\frac{d\mathrm{x}}{d\lambda}\left(n_s \frac{D}{L_f}\right) + \frac{dn_s}{d\lambda}\left(\mathrm{x}\frac{D}{L_f}\right) + \frac{dn_c}{d\lambda}\Delta \mathrm{L} = \mathrm{m} \tag{6}$$

$$\lambda_0 = \frac{n_c\, \Delta \mathrm{L}}{m} \tag{7}$$

If the focus point with diffraction angle Øe is defined as E and the distance between S and E as x, then the wavelengths $\lambda$ and x are expressed as:

$$\frac{dx}{d\lambda} = \frac{L_f \, \Delta L}{n_s \, D\lambda_0} \, n_g \tag{8}$$

where $L_f$ is the focal length of the slab waveguide; $D$ is the pitch of adjacent arrayed waveguide; $n_s$ is the effective refractive index of the slab waveguide; and $n_g$ is the group refractive index of the arrayed waveguide.

Equation (8) shows the linear dispersion of the AWG, showing that when the input waveguide is at a distance dx from S, it can input light with a different wavelength from $\lambda_0$ by $d\lambda$. The input waveguide moves a distance corresponding to the wavelength change $d\lambda$ to compensate for the temperature change and the temperature dependence of the center wavelength. To implement this principle, this study applied a new concept that separates one of the slab waveguides.

Figure 3 shows the structure of this new athermal AWG. The AWG's circuit cuts one slab waveguide and separates it into a large part and a small part. These two parts are attached to the temperature compensation board (Invar), which acts as a compensation plate, and the temperature is compensated by the thermal expansion coefficient of SUS 304 bolts. These bolts are connected to both ends of the temperature compensation board.

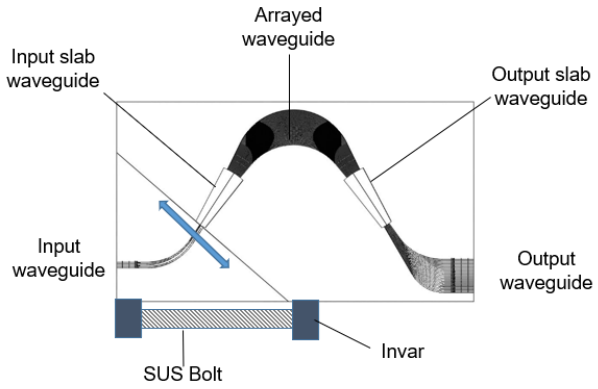


**Figure 3.** Structure of athermal AWG.

Figure 4 shows the temperature compensation mechanism. In conventional AWGs, the focus point shifts according to temperature change, and the center wavelength of AWG varies with temperature.

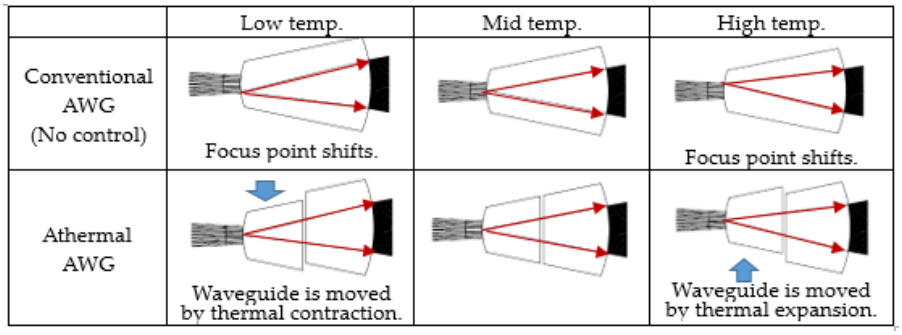


**Figure 4.** Mechanism of athermal AWG.

However, in an athermal AWG, the focus point also shifts according to temperature change, but the center wavelength remains constant because the output waveguide moves to the shifted focus point by the thermal contraction and expansion of SUS 304 bolts. This temperature compensation mechanism also applies when light is input from the output

port. Athermal AWG uses a technology to control the focus in slab waveguides, so it is not temperature sensitive and has an insignificant effect on optical properties. This implements an athermal AWG with many channels. The compensation is also very stable because the thermal expansion coefficient of the SUS304 bolts is constant and very stable.

To accurately compensate for the temperature dependence of the athermal AWG's center wavelength, the distance of the temperature compensation board, determined as follows, should be adjusted by referring to the parameters in Table 1.

**Table 1.** Circuit parameters of AWG.

| Parameter | Values |
|---|---|
| Channel spacing | 50 GHz |
| Number of channels | 96 |
| Focal length of slab waveguide: $L_f$ | 26,751 μm |
| Path length difference of arrayed waveguide: $\Delta L$ | 30.84 μm |
| Pitch of adjacent arrayed waveguide: $D$ | 8.5 μm |
| Group index of arrayed waveguide at R.T.: $n_g$ | 1.480 |
| Effective index of slab waveguide at R.T.: $n_s$ | 1.454 |

The change in position compensation dx can be expressed as a function of temperature change.

$$dx = \left( \frac{L_f \, \Delta L}{n_s \, D\lambda_0} \, n_g \right) d\lambda \tag{9}$$

$$\frac{dx}{dT} = \left( \frac{L_f \, \Delta L}{n_s \, D\lambda_0} \, n_g \right) \frac{d\lambda}{dT} \tag{10}$$

Equation (11) below is derived by using the parameters in Table 1.

$$\frac{dx}{dT} = 0.280 \, \frac{\mu m}{deg} \tag{11}$$

That is, when the temperature changes by 1 °C, the focus point must change by 0.280 μm/deg in the input end of the input slab waveguide.

Therefore, the temperature compensation board needs to compensate for this value.

The thermal expansion coefficient of the SUS304 bolts is $1.73 \times 10^{-5}$/°C, so the distance of the temperature compensation board becomes 48.55 mm, according to the design of AWG.

## 3. Athermal AWG Fabrication Results

Based on the principle of temperature compensation and patent described above, a compact athermal AWG module Gaussian-type (130 mm × 90 mm × 11 mm) was fabricated using 96-channel (50 GHz-spacing) athermal AWG chip technology and PLC manufacturing technology, as shown in Figure 5 below.


**Figure 5.** Appearance of athermal AWG module.

Based on Telcordia GR-1221-CORE [19] and Telcordia-GR-1209-CORE [20] for passive optical components, reliability tests were performed on athermal AWG modules under the conditions in Table 2 to measure the performance characteristics before and after the test at room temperature.

**Table 2.** Reliability test conditions.

| Item | Condition [19] |
| --- | --- |
| Vibration | 20 G, 20~2000 Hz<br>4 min/cycles, 4 cycles/axis, 3 axis |
| Cycling moisture Resistance test | 25 °C~65 °C, 80%~100% R.H. |
| Temperature cycling test | −10 °C, 10 cycles<br>−40 °C~85 °C, 500 cycles |
| High-temperature storage test | 85 °C, 2000 h |
| Low-temperature storage test | −40 °C, 2000 h |

Five samples were used for each reliability test to compare the center wavelength and insertion loss values before and after the tests at room temperature. Figure 6 shows the spectra over all channels for the 96-channel (50 GHz-spacing) athermal AWG modules and the spectrum of one of the samples before the test.

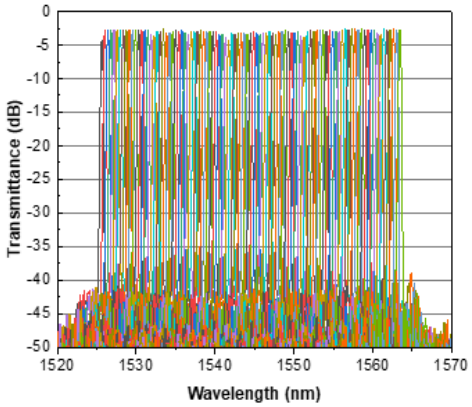


**Figure 6.** Spectrum of athermal AWG.

Figure 7 shows the wavelength and the loss variation measured and monitored during the temperature cycling test. The center wavelength shift and insertion loss values of channels 1, 48, and 96 were measured in the temperature cycling test (−40 °C~85 °C). Figure 7a shows the temperature dependence of the center wavelength for three wavelengths (1 ch., 48 ch., 96 ch.) of the 96-channel (50 GHz-spacing) athermal AWG module, confirming that the temperature was compensated. Figure 7b shows the temperature dependence of spectrum 48 ch., in which the center wavelength shift at 85 °C was ±0.05 nm. Figure 7c shows the temperature dependence of the center wavelength for the AWG module (1 ch., 48 ch., 96 ch.) between −40 °C~85 °C, in which the temperature compensation was less than ±0.05 nm. Figure 7d shows that the insertion loss variation was less than ±0.5 dB in the range of −40 °C~85 °C.

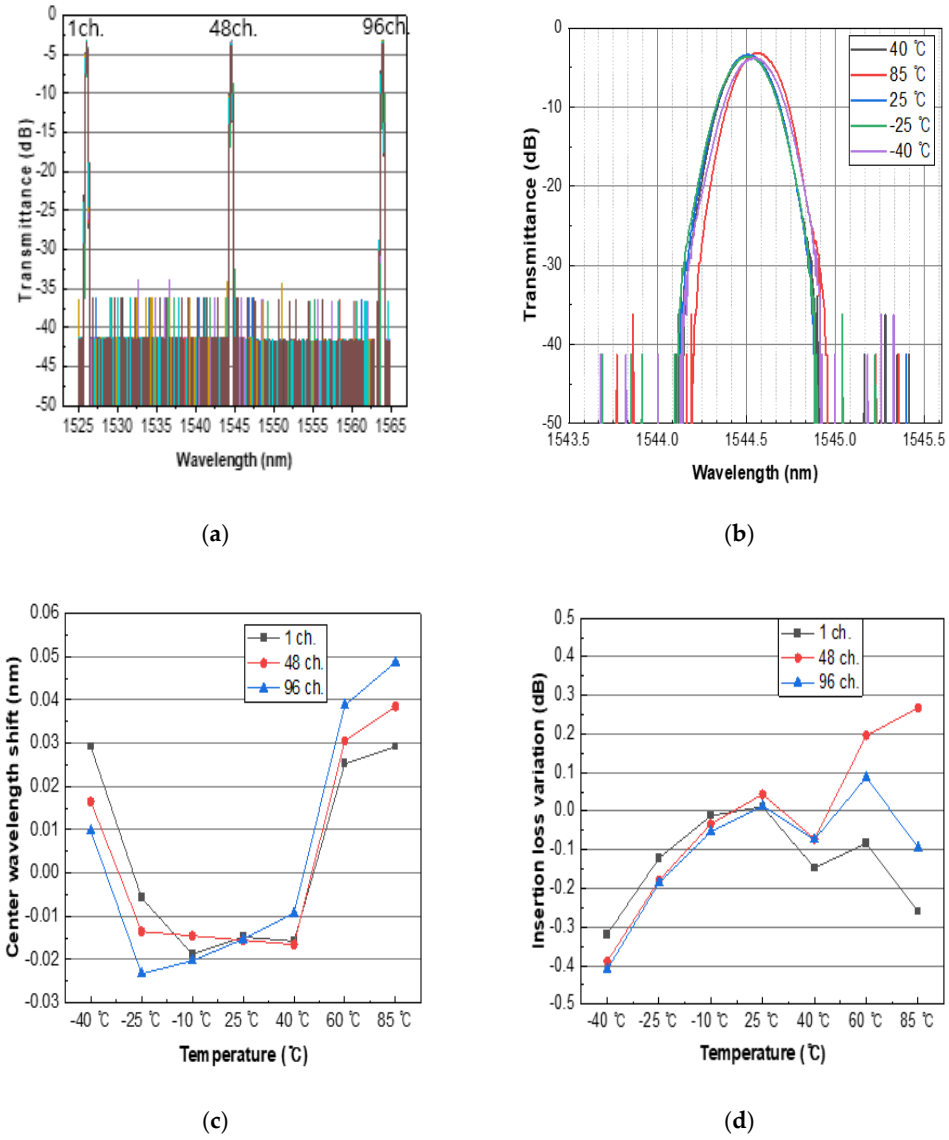


**Figure 7.** Temperature dependence of 96-channel (50 GHz-spacing) athermal AWG: (**a**) Temperature dependence of center wavelength; (**b**) Temperature dependence of spectrum 48 ch; (**c**) Center wavelength shift of Temperature dependence; (**d**) Insertion loss variation of temperature dependence.

## 4. Reliability Test Result for Outdoor Environments Application

Based on Telcordia-GR-1221-CORE [19] and Telcordia-GR-1209-CORE [20] for passive optical components, reliability tests were performed on the 96-channel (50 GHz-spacing) athermal AWG modules under the conditions in Table 3 to obtain the results. Five samples were used for each reliability test item to measure and compare the center wavelength, insertion loss values, and insertion loss variation before and after the tests at room temperature.

According to the reliability test results in Table 3, the maximum insertion loss change was within ±0.19 dB, which satisfies the 0.5 dB or 10% requirements of Telcordia-GR-1221-CORE. The average insertion loss is the average value of the 1 to 96 channels of five samples tested separately and was within a maximum of −3.72 dB, which is less than the Telcordia-GR-1209-CORE reference of 6.14 dB.

Among the five reliability tests, the insertion loss average of the low-temperature storage test showed the greatest loss of −3.54 dB. The average insertion loss changes of the five reliability items were between −0.08 dB and 0.03 dB, indicating that the performance was stable even after the reliability tests without significant differences.

**Table 3.** Reliability test results.

| Item | Condition [19] | *n* | Results | | |
|---|---|---|---|---|---|
| | | | Average Center Wavelength Change (nm) | Average Insertion Loss Change (dB) | Average Insertion Loss (dB) |
| Vibration | 20 G, 20~2000 Hz 4 min/cycles, 4 cycles/axis, 3 axis | 5 | All Ch. 0.003<br>1 ch. 0.001<br>96 ch. 0.000 | All Ch. 0.03<br>1 ch. −0.01<br>96 ch. 0.19 | −3.33<br>−3.51<br>−3.39 |
| Cycling moisture Resistance test | 25 °C~65 °C, 80%~100% R.H. −10 °C, 10 cycles | 5 | All Ch. 0.006<br>1 ch. 0.005<br>96 ch. 0.008 | All Ch. −0.02<br>1 ch. −0.05<br>96 ch. 0.04 | −3.26<br>−3.23<br>−3.56 |
| Temperature cycling test | −40 °C~85 °C, 500 cycles | 5 | All Ch. 0.011<br>1 ch. 0.011<br>96 ch. 0.009 | All Ch. −0.08<br>1 ch. −0.04<br>96 ch. −0.04 | −3.34<br>−3.27<br>−3.60 |
| High-temperature storage test | 85 °C, 2000 h | 5 | All Ch. 0.020<br>1 ch. 0.022<br>96 ch. 0.020 | All Ch. −0.03<br>1 ch. 0.19<br>96 ch. −0.08 | −3.36<br>−3.32<br>−3.46 |
| Low-temperature storage test | −40 °C, 2000 h | 5 | All Ch. 0.006<br>1 ch. 0.003<br>96 ch. 0.007 | All Ch. −0.05<br>1 ch. 0.03<br>96 ch. −0.13 | −3.54<br>−3.25<br>−3.72 |

Figure 8 shows the 96-channel average data of five AWG modules after the temperature cycling test. Figure 8a shows the center wavelength shift, and Figure 8b the insertion loss variation. After testing 500 cycles (−40 °C~85 °C), the center wavelength shift was within ±0.022 nm and the insertion loss variation within ±0.22 dB, which is stable against temperature changes.

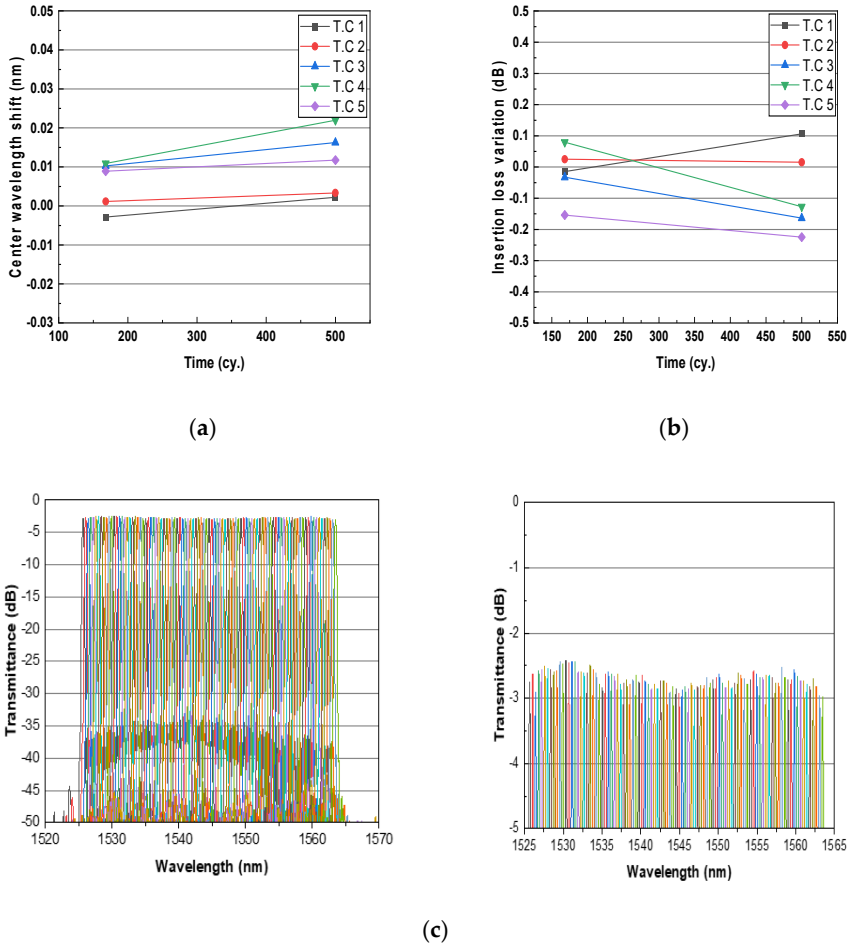


**Figure 8.** All channel average result of module after temperature cycling test: (**a**) Center wavelength shift; (**b**) Insertion loss variation; (**c**) Spectrum after temperature cycling test (T.C 1).

Figure 9 shows the 96-channel average data of five AWG modules after the high-temperature storage reliability test at 85 °C for 2000 h. The center wavelength shift was within ±0.060 nm, and the insertion loss variation was within ±0.15 dB, which is stable for a long time under a high-temperature environment.

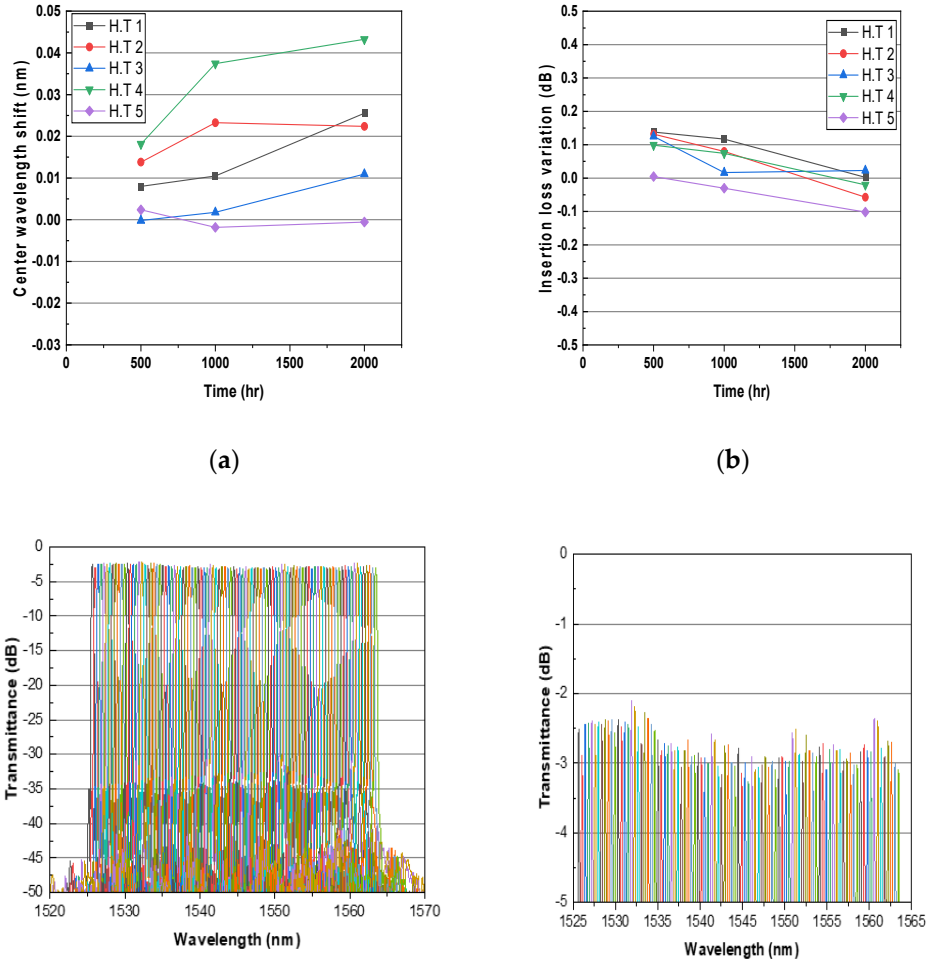


**Figure 9.** All channel average result of module after high storage temperature test: (**a**) Center wavelength shift; (**b**) Insertion loss variation; (**c**) Spectrum after high storage temperature test (H.T 1).

Figure 10 shows the 96-channel average data of five AWG modules after the low-temperature storage reliability test at −40 °C for 2000 h. The center wavelength shift was within ±0.030 nm, and the insertion loss variation was within ±0.35 dB, which is stable for a long time under a low-temperature environment.

The reliability test results of five items including vibration, temperature cycling, and high-temperature storage tests prove that the 96-channel (50 GHz-spacing) athermal AWG module is highly reliable without failure and ensures its reliability for long-term use in optical communication networks.

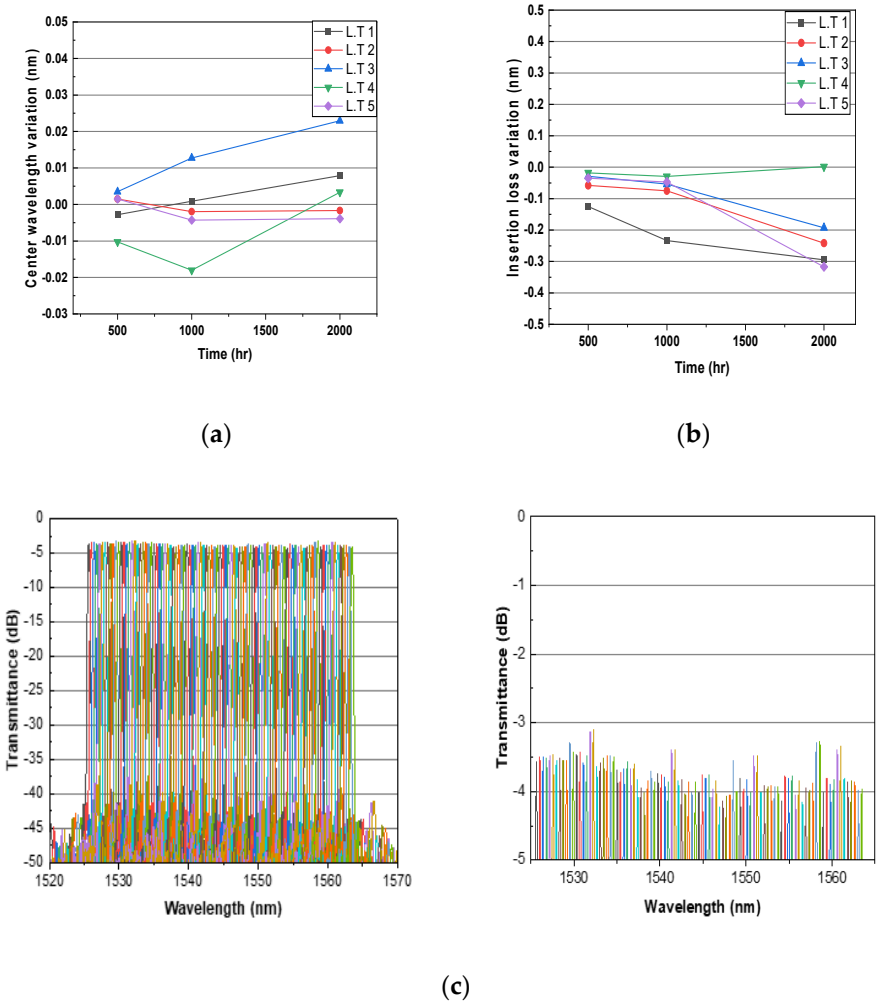


**Figure 10.** All channel average result of module after low storage temperature test; (**a**) Center wavelength shift; (**b**) Insertion loss variation; (**c**) Spectrum after low storage temperature test (L.T 1).

## 5. Lifetime Estimation

### *5.1. Accelerated Life Test*

Accelerated life tests were performed along with the reliability tests to predict the service life of the 96-channel (50 GHz-spacing) athermal AWG. The test estimated the life-stress relationship using the Arrhenius equation by elevating temperatures according to the Meeker and Hahn plan (optimized 4:2:1 allocation), which considers stress extrapolation and time extrapolation to increase the accuracy of lifetime prediction [21].

#### 5.1.1. Preparation

Based on the accelerated life test conditions in Table 4, the samples were measured at 250-h intervals for 4000 h using three high-temperature chambers (ESPEC), an optical source (Amonics), and an Optical Spectrum Analyzer (Anritsu, MS9740A) at three different temperatures, 71 °C, 83 °C, and 95 °C. The failure criteria were based on accidental failure or a 50% change in the initial measurement. Data reliability was improved by measuring channels 1 and 48. A total of 28 samples (Gaussian type 21, Flat type 7) were distributed by temperature.

**Table 4.** Test conditions.

| Temperature °C | *n* |
|---|---|
| 71 | 16 |
| 83 | 8 |
| 95 | 4 |

5.1.2. Accelerated Life Test Model

As shown in Table 5, the likelihood function values of the Weibull distribution, lognormal distribution, and exponential distribution were compared using ALTA S/W to find a suitable distribution for the data measured for 4000 h during the accelerated life test. As a result, the lognormal distribution, which had the largest likelihood function value, was the most suitable lifetime distribution.

**Table 5.** Conformance result of life distribution.

| Distribution | L.K |
|---|---|
| Exponential | −44.37 |
| Lognormal | −43.94 |
| Weibull | −44.49 |

Figure 11 shows the failure data observed in the accelerated life test using ALTA S/W. Since the data of each test condition are close to a straight line and the lifetime distribution estimation line is parallel, the lognormal distribution is suitable, and acceleration is established between the test conditions.

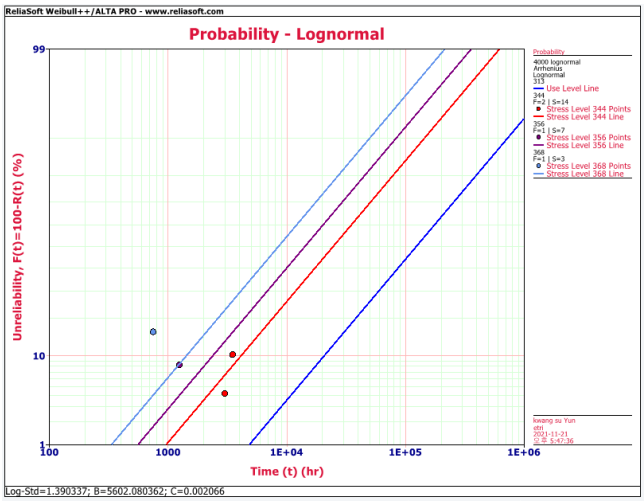


**Figure 11.** Lognormal probability plot.

5.1.3. Lognormal Distribution and Life–Stress Relationship

The life distribution model was based on a lognormal distribution, and the life–stress relationship uses the Arrhenius relationship, which is widely used in accelerated life tests by temperature, as shown in Equation (12) below.

$$\zeta(T) = A \cdot \exp\,[E/(kT)] \quad (12)$$

where $\zeta(T)$ is the lifetime distribution parameter; E is the activation energy (eV); k is the Boltzmann constant ($8.617 \times 10^5$ eV/°C); T is the absolute temperature (K, °C + 273.15); and A is a constant according to the material properties and test conditions.

The acceleration factor (AF) from the life–stress relationship is shown in Equation (13) below.

$$AF = \zeta(T_d)/\zeta(T_a) = \exp\left[(E/K)\cdot(1/T_d - 1/T_a)\right] \quad (13)$$

where $T_d$ is the lifetime under operating conditions, and $T_a$ is the lifetime under accelerated conditions.

The activation energy (Ea) estimated from the software was 0.482. Therefore, as a result of calculating the acceleration factors for each acceleration stress, as shown in Figure 12, the life–stress relationship for temperatures 71 °C, 83 °C, and 95 °C shows that the lifetime reduced as the temperature increased.

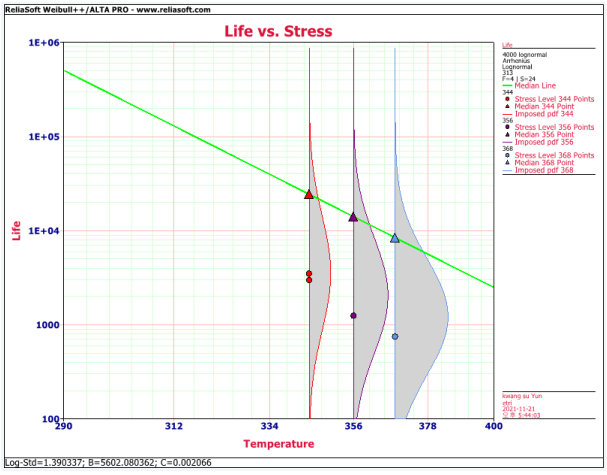


**Figure 12.** Life vs. stress.

### *5.2. Accelerated Life Test Results*

Table 6 shows the failures that occurred under the temperature conditions during the accelerated life test for 4000 h. The samples consisted of 28 96-channel (50 GHz-spacing) athermal AWGs (Gaussian type 21, Flat type 7). Four failures occurred only in the Gaussian type. After the accelerated life test, the insertion loss for each channel of each representative sample was measured, as shown in Figure 13. After the high-temperature acceleration test, the average insertion loss was −4.35 dB at 71 °C, −4.89 dB at 83 °C, and −4.68 dB at 95 °C, and the higher the temperature, the greater the loss tends to be.

**Table 6.** Results after the accelerated life test.

| Temperature °C | *n* | Fail | Fail Time |
|---|---|---|---|
| 71 | 16 | 2 | 3000 h, 3500 h |
| 83 | 8 | 1 | 1250 h |
| 95 | 4 | 1 | 750 h |

Although the high-temperature accelerated life test lasted for 4000 h, it satisfied the Telcordia-GR-1209 standards and showed reliability in wavelength.

The accelerated tests on the athermal AWG module under high-temperature stress followed a lognormal distribution. The activation energy calculated by ALTA S/W was 0.482 eV, and the predicted mean life under 40 °C operating conditions was up to $3.22 \times 10^5$ (about 36.7 years), which guarantees the 10-year service life required for optical communication components. Although an accelerated life test of 4000 h was performed at high temperature, the wavelength showed reliability.

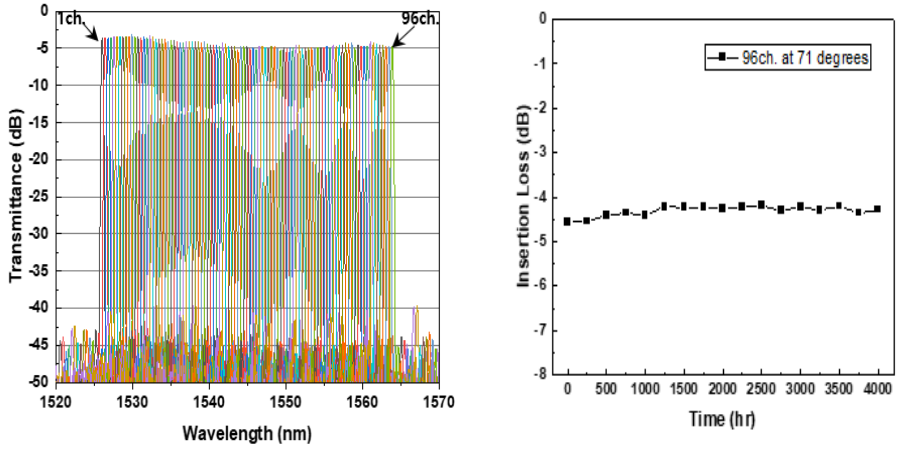


(**a**)

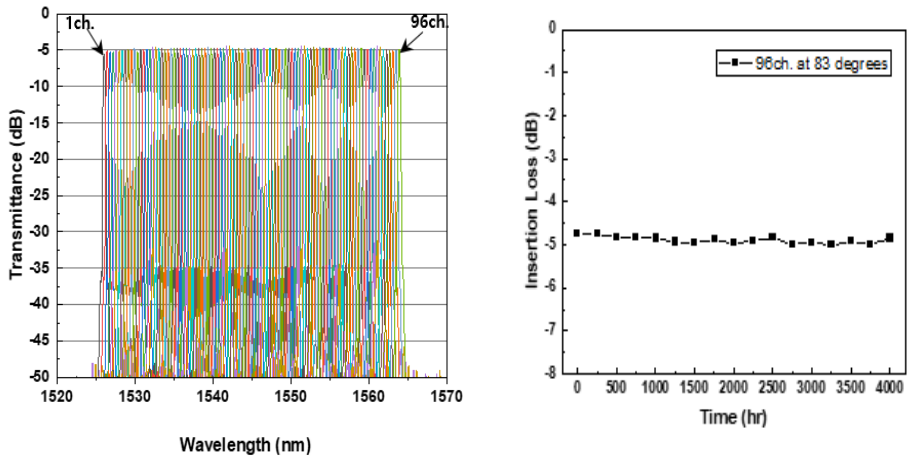


(**b**)

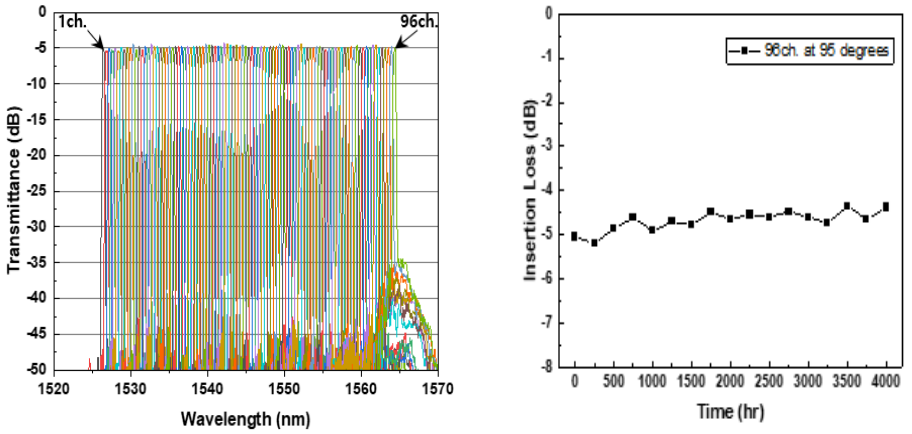


(**c**)

**Figure 13.** Transmittance and insertion loss changes after accelerated life test; (**a**) Transmittance and insertion loss for each wavelength at 71 °C; (**b**) Transmittance and insertion loss for each wavelength at 83 °C; (**c**) Transmittance and insertion loss for each wavelength at 95 °C.

## 6. Conclusions

The temperature dependence of the center wavelength in the 96-channel (50 GHz-spacing) athermal AWG module developed based on a new temperature compensation

board shape and patent satisfied the ±0.05 nm range in all channels in the temperature range of −40 °C~85 °C, and the insertion loss variation was also less than ±0.5 dB.

As a result of performing reliability tests based on Telcordia-GR-1209 and GR-1221, the temperature dependence of the center wavelength satisfied the ±0.022 nm range, and the insertion loss variation was also less than ±0.2 dB. According to the accelerated life test by high-temperature stress, the predicted mean life of the AWG module was $3.22 \times 10^5$ (about 36.7 years), which is more than enough to guarantee the 10-year service life required for optical communication components.

The developed athermal AWG module showed sufficient performance and reliability to be applied to 5G mobile networks such as reducing the power consumption and volume of DWDM network systems and enabling easy management.

**Author Contributions:** Conceptualization, K.-S.Y., C.-H.Y. and I.J.; Software, K.-S.Y.; Formal analysis, K.-S.Y., Y.-S.K.; Data curation, K.-S.Y., Y.-S.K.; Writing, K.-S.Y.; Review, K.-S.Y., C.-H.Y., K.-S.L., Y.-S.K. and I.J.; Visualization, K.-S.Y.; Funding acquisition, K.-S.L., I.J. All authors have read and agreed to the published version of the manuscript.

**Funding:** This research was financially supported by an Electronics and Telecommunications Research Institute (ETRI) grant funded by the Korean government [21RK1100, (Honam Area) Post Pandemic Regional Strategic Industry Support Project] and Chonnam National University (Grant number: 2020-3815).

**Institutional Review Board Statement:** Not applicable.

**Informed Consent Statement:** Not applicable.

**Data Availability Statement:** Not applicable.

**Conflicts of Interest:** The authors declare no conflict of interest.

## References

1. Pandey, G.; Choudhary, A.; Dixit, A. Wavelength division multiplexed radio over fiber links for 5G fronthaul networks. *IEEE J. Sel. Areas Commun.* **2021**, *39*, 2789–2803. [CrossRef]
2. Chen, B.; Hong, D.; Wang, L.; Ou, Y.; Tan, Y.; Li, X.; Zhong, X. A high-reliability optical network architecture based on wavelength division multiplexing passive optical network. *Optoelectron. Lett.* **2021**, *17*, 422–426. [CrossRef]
3. Grobe, K.; Elbers, J.P. Analysis of WDM-PON for next-generation back-and fronthaul. In *Broadband Coverage in Germany; 10. ITG-Symposium*; VDE: Berlin, Germany, 2016; pp. 1–5.
4. Han, J.; Han, P.; Liu, Y. Survivable Wavelength-Division-Multiplexed Passive Optical Network for Fronthaul in 5G and Beyond. In Proceedings of the 2021 9th International Conference on Intelligent Computing and Wireless Optical Communications (ICWOC), IEEE, Chongqing, China, 4–7 June 2021.
5. Amiri, I.S.; Houssien, F.M.A.M.; Rashed, A.N.Z.; Mohammed, A.E.N.A. Comparative simulation of thermal noise effects for photodetectors on performance of long-haul DWDM optical networks. *J. Opt. Commun.* **2019**. [CrossRef]
6. Sadinov, S.M.; Angelov, K.K.; Kogias, P. Modelling and performance analysis of DWDM passive optical network. In *IOP Conference Series: Materials Science and Engineering*; IOP Publishing: Bristol, UK, 2021; Volume 1032.
7. Mubarakah, N.; Fadhilah, D.D. Point to Point Communication Link Design by Using Optical DWDM Network. In Proceedings of the 2020 4rd International Conference on Electrical, Telecommunication and Computer Engineering (ELTICOM), IEEE, Medan, Indonesia, 3–4 September 2020.
8. Blumenthal, D.J.; Heideman, R.; Geuzebroek, D.; Leinse, A.; Roeloffzen, C. Silicon nitride in silicon photonics. *Proc. IEEE* **2018**, *106*, 2209–2231. [CrossRef]
9. Fan, Z.; Zhao, J.; He, J.J. High Performance Demonstration of a 16 × 16 Silica-based Cyclic Arrayed-Waveguide Grating Router. In Proceedings of the 2021 19th International Conference on Optical Communications and Networks (ICOCN), IEEE, Qufu, China, 23–27 August 2021.
10. Lohrmann, R.; 4 Filters for CWDM WDM. Coarse Wavelength Division Multiplexing: Technologies and Applications. CRC Press: London, UK, 2018; p. 91.
11. Bucio, T.D.; Khokhar, A.Z.; Mashanovich, G.Z.; Gardes, F.Y. Athermal silicon nitride angled MMI wavelength division (de) multiplexers for the near-infrared. *Opt. Express* **2017**, *25*, 27310–27320. [CrossRef] [PubMed]
12. Wu, X.; Liu, C.; Liu, W.; Li, C.; Yuan, Z.; Guan, C.; Wu, K.; Tang, F.; Min, Y.; Chen, H.; et al. Integrated athermal arrayed-waveguide grating multiplexer and demultiplexer with all-metal compensating rod for broadband temperature application. *Appl. Opt.* **2018**, *57*, 6207–6212. [CrossRef] [PubMed]

13. Melati, D.; Verly, P.G.; Delâge, A.; Cheben, P.; Schmid, J.H.; Janz, S.; Xu, D.X. Athermal echelle grating filter in silicon-on-insulator using a temperature-synchronized input. *Opt. Express* **2018**, *26*, 28651–28660. [CrossRef] [PubMed]
14. Leick, L.; Boulanger, M.; Nielsen, J.G.; Imam, H.; Ingenhoff, J. Athermal AWGs for colourless WDM-PON with −40 °C to +70 °C and underwater operation. In Proceedings of the Optical Fiber Communication Conference and Exposition and the National Fiber Optic Engineers Conference, Anaheim, CA, USA, 5–10 March 2006; Optical Society of America: Washington, DC, USA.
15. Wang, M.; Chen, X.; Guan, C.; Yu, J. Monolithic integrated athermal arrayed-waveguide grating multiplexer and demultiplexer. In *Fiber Optic Sensing and Optical Communication*; International Society for Optics and Photonics: Beijing, China, 2018; p. 1084902.
16. Ticknor, A.J.; McGinnis, B.P.; Tarter, T. Efficient passive and active wavelength-stabilization techniques for AWGs and integrated optical filters. In Proceedings of the Optical Fiber Communication Conference and Exposition and the National Fiber Optic Engineers Conference, Anaheim, CA, USA, 6 March 2005; Optical Society of America: Washington, DC, USA.
17. Hasegawa, J.; Nara, K. Ultra-wide temperature range (−30~70 °C) operation of athermal AWG module using pure aluminum plate. In Proceedings of the Optical Fiber Communication Conference and Exposition and the National Fiber Optic Engineers Conference, Anaheim, CA, USA, 5–10 March 2006; Optical Society of America: Washington, DC, USA, 2006.
18. Zheng, Y.; Wu, Y.; Sun, H.; He, H.; Liu, Z. Optical performances analysis and structure parameters optimization design of dense arrayed waveguide grating. *Results Opt.* **2021**, *2*, 1000049. [CrossRef]
19. Telcordia-GR-1221-CORE. Generic Reliability Assurance Requirements for Passive Optical Components. 2010. Available online: https://telecom-info.njdepot.ericsson.net/site-cgi/ido/docs.cgi?ID=SEARCH&DOCUMENT=GR-1221&#ORD (accessed on 9 October 2021).
20. Telcordia-GR-1209-CORE. Generic Requirements for Passive Optical Components. 2010. Available online: https://telecom-info.njdepot.ericsson.net/site-cgi/ido/docs.cgi?ID=SEARCH&DOCUMENT=GR-1209& (accessed on 9 October 2021).
21. Meeker, W.Q.; Hahn, G.J. *How to Plan an Accelerated Life Test: Some Practical Guidelines*; Statistical Techniques; ASQC Quality Press: Milwaukee, WI, USA, 1985; Volume 10.